行政院國家科學委員會補助專題研究計畫 ■ 成 果 報 告 □期中進度報告

（計畫名稱）

表面原子尺度建造之自旋的第一原理計算

計畫類別：■個別型計畫　□整合型計畫
計畫編號：NSC 97－2112－M－009－007－MY3
執行期間：97 年 08 月 01 日至 100 年 07 月 31 日

執行機構及系所：國立交通大學 電子工程學系及電子研究所

計畫主持人：林炯源
共同主持人：
計畫參與人員：劉勝元、謝尚恒、謝耀賢、姚景能、林庭煦、黃威智

成果報告類型(依經費核定清單規定繳交)：□精簡報告　■完整報告

本計畫除繳交成果報告外，另須繳交以下出國心得報告：
□赴國外出差或研習心得報告
□赴大陸地區出差或研習心得報告
■出席國際學術會議心得報告
□國際合作研究計畫國外研究報告

處理方式：除列管計畫及下列情形者外，得立即公開查詢
□涉及專利或其他智慧財產權，□一年□二年後可公開查詢

中　華　民　國 100 年 10 月 31 日

(二)中、英文摘要及關鍵詞

為邁向原子尺度磁系統元件應用的道路，我們與 IBM 矽谷研究中心的掃描穿隧顯微鏡實驗室合作，在特別的表面建造磁原子結構。該表面是在銅(100)上覆蓋單層氮化銅。此獨一設計使吸附原子的自旋免受傳導電子的遮蔽，又容許足夠的穿隧電流從掃描探針通到表面來探測自旋激發，並更進一步讓探針對個別原子進行建構、探測與改造。為了製成具有較強磁性的表面原子尺度結構，以下有三個重要課題：計算並調控自旋間的耦合、探索單一原子自旋的異向性、自旋的耦合與異向性之相互影響。第一個課題關係到大磁化量原子尺度結構的製成，該製成乃藉由將上述表面建造的原子自旋進行鐵磁耦合。第二者能藉由鎖定原子自旋的方向來幫助建構磁儲存位元。最後是進一步於原子尺度發展出巨大磁異向性。研究此一新穎磁系統的方法是相當性先進的密度汎函理論搭配擴增平面波法。我們首先將尋找具有鐵磁耦合的原子自旋系統並從中學習如何藉由不同吸附磁原子與排列幾何來改變耦合強度，我們預期會找到數個合適的原子與排列幾何，並用計算這些不同系統的自旋耦合及其他磁性特質。我們也將計算不同吸附磁原子的自旋異向性，並以具有 f 軌域者為優先。我們也將研究不同軌道角動量對自旋異向性的影響。把數個具有自旋異向性的原子耦合成為較大的量子自旋結構，將有助於在原子尺度建構出巨大磁異向性。我們將會在表面放置同時具有自旋耦合與自旋異向性的原子，並研究這兩個效應在共存時如何相互影響。

關鍵詞：掃描穿隧顯微鏡、自旋耦合、自旋異向性、第一原理、密度汎函理論。

We collaborated with the STM Lab at IBM Almaden Research Center in engineering magnetic atoms on a specially designed surface, an insulating CuN monolayer on top of the Cu(100) surface. This unique design provides the opportunity to preserve the spins of magnetic adatoms from being screened by the underlying conduction electrons while at the same time allowing enough tunneling current from an STM tip to probe the spin excitations. Moreover, the magnetic atoms on this surface can be constructed, probed, and manipulated atom-by-atom. In order to fabricate surface-embedded atomic-scale structures with strong magnetism, there are three important topics: How strong is the coupling between two spins on this surface and how can the coupling strength be tuned? What is the detailed structure of the anisotropy of a single atomic spin and how can one possibly control such anisotropy? What is the interplay between the spin coupling and anisotropy? The first topic is related to fabricating of atomic-scale structures with a large spin on a surface by coupling those atomic spins ferromagnetically. The second helps construct magnetic storage bits by aligning individual atomic spins. The last can enable further development of giant magnetic anisotropy at the atomic scale. DFT in the FLAPW basis will be used to study the magnetic properties of such novel systems. We will first search for magnetic adatoms that exhibit ferromagnetic coupling between their spins by changing geometries. The

magnetic anisotropy is responsible for the orientation of spins. We will also calculate spin anisotropy of various different magnetic adatoms on the same surface, presumably magnetic atoms with *f* orbitals. We will place on the CuN surface the magnetic atoms that exhibit both spin coupling and anisotropy. The interplay of these two effects upon their coexistence in engineered spin systems will be studied.

Keywords: STM, atomic spin coupling, spin anisotropy, first-principles, density functional theory.

(三)報告內容：

1. 前言 2. 研究目的 3. 文獻探討

Magnetism is becoming very important area in new technology in industry primarily because of data storage. Hard drives and video-audio tapes are the two most familiar types of magnetic-storage media in our daily lives. Magnetism also surprisingly is being used now in computation. There is a recent paper at *Science* **309**, 2180 (2005) that demonstrates how spins in quantum dots are coupled to form qbits (Fig. 1 left). Moreover, one can also perform classical computation with magnetism: as shown in another paper *Science* **311**, 205 (2006), several small lithographically fabricated ferromagnetic islands are coupled to perform logical operation (Fig. 1 right). Magnetism is also very interesting from both physics and

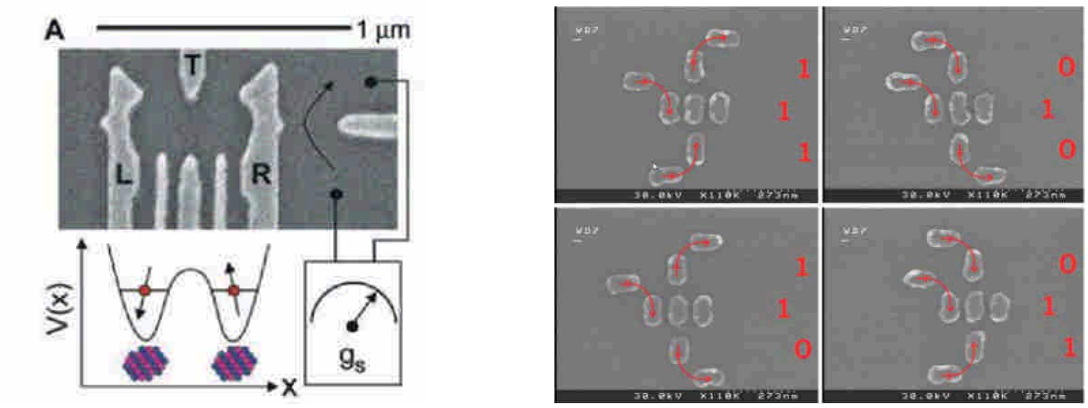

Figure 1: The left figure shows a double quantum dot acting as two coherent spin states. The system allows state preparation, coherent manipulation, and projective readout, and forms a long-lasting qubit. The right figure shows three magnets (red arrows), with the central one to be antiferromagnetic and the other two ferromagnetic, form logical gates according to their resulting magnetization directions due to a horizontal magnetic field.

chemistry points of view. Physicists have been able to make a set of lithographically fabricated ferromagnetic islands in a regular array, where the array is arranged such that its Hamiltonian is the same as the spin ice. Spin ice has a very degenerate ground state, and allows all sorts of interesting magnetic quantum properties. The advantage of this vs. the standard bulk- material people use to study spin ice is that this is fabricated by hand. Chemists can also couple a small number of atomic spins together in various structures, the well-known molecular magnets. The stereotypical molecular magnet is the Mn 4- acetate that has 12 Mn atoms in a large structure (see Fig. 2), first reported at *Acta Crystallogr. Soc.* B **36**, 2042 (1980). The structure of a molecular magnet can be controlled such that it has rather large net spin. In summary, there are two methodologies of making nanoscale magnets: the top-down approach (spin ice) where one sprinkles a lot of atoms down to the surface. This method is very good for manipulating structures, but unfortunately it has not reached atomic-scale control. On the other hand if one uses the bottom-up approach like in chemistry, there is atomic-scale control, but the structure cannot be easily manipulated after being built. There is a recent development by the low-temperature STM group at IBM Almaden Research Center that applies a technique somewhere in between the spin-ice and molecular-magnet approaches in making nanoscale magnets. This group has been pioneering in manipulating individual atoms on material surfaces. The earliest work was being able to spell out the letters I-B-M with individual Xe atoms in 1989, perhaps the most important landmark of nanoscience. The continuous works, Quantum Corral and Quantum Mirage, have drawn so much attention of the scientific society and were published at *Science* **262**, 218 (1993) and *Nature* **403**, 512 (2000) respectively.

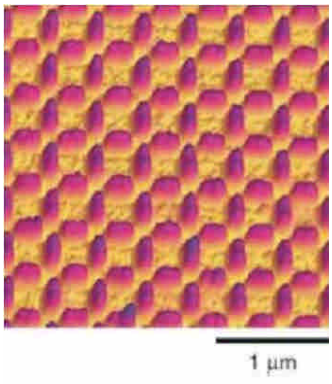

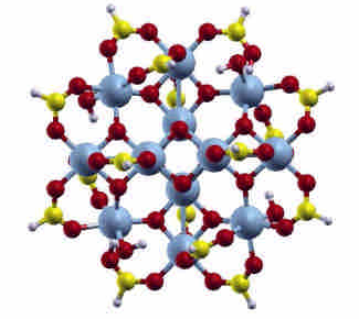

Figure 2: The left is a lithographically fabricated spin ice. The right is the ball-and-stick model of Mn12-ac, with methyl groups replaced for clarity by hydrogen atoms (large balls are Mn atoms).

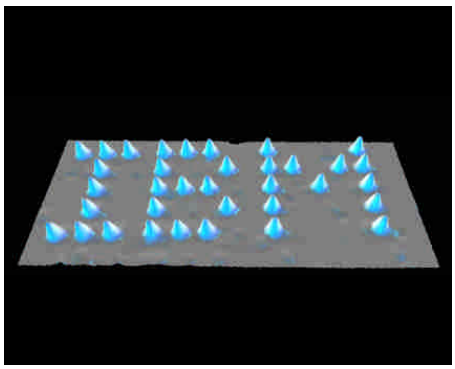

Figure 3: Spelling out the letters "I-B-M" using 35 Xe atoms on a Ni (110) surface.

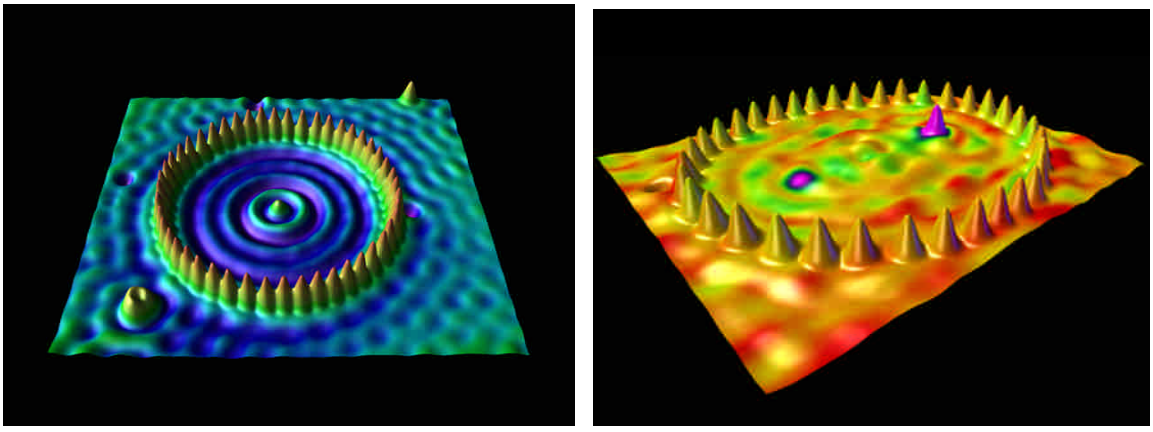

Figure 4: The left shows an STM image of direct observation of standing-wave patterns in the local density of states of the Cu(111) surface, called Quantum Corral. The circular corral of radius 71.3Å was constructed out of 48 Fe adatoms. The right shows that an elliptic corral projects the electronic states of the surface electrons surrounding the focal cobalt atom to the other focus of the ellipse that has no magnetic atom, called Quantum Mirage.

Their advance in atom manipulation on surfaces has recently made it possible to probe magnetism of individual atoms, as well as demonstrated that STM can build chains of Mn atoms and measure magnetic excitation of such chains using Inelastic Tunneling Spectroscopy (IETS), reported at Science **312**, 1021 (2006). This new technique can be used to explore the limits of magnetic data storage, by engineering the energy required to flip the collective orientation of a small number of magnetically coupled atoms. *Physics Today* calls this achievement as "a proof-of principle demonstration that sets the stage for creating

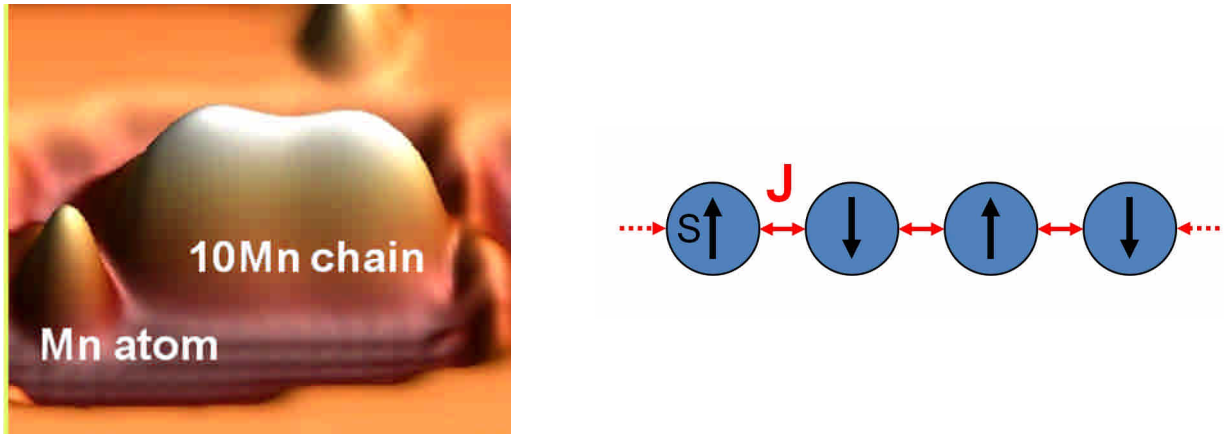

Figure 5: The left shows the perspective rendering of a chain of 10 Mn atoms. The right shows the schematic of the antiferromagnetically coupled atomic spins described by the Heisenberg model.

designer magnets, from Heisenberg spin chains to exotic spin ices". An applied-physics perspective in the *Science Magazine* comments, "Understanding magnetic ordering at the atomic scale is essential for spintronic technology. A linear chain of manganese atoms has been created for studying one-dimensional systems." *Nature Materials* claims that the study "has shown that it is possible to assemble quantum spin structures on a surface, but they also provided a method of reading and modifying their spin states to investigate the most fundamental magnetic interactions in matter." In this purely experimental study, there are several questions that are not answered: Is the spin coupling mediated by the underlying conduction electrons or the N atoms? How does the absorption of the Mn atoms affect the chemical properties of the substrate, e.g. the inter-atomic polarity? Can one find ferromagnetic coupling in a similar system (Mn chains are antiferromagnetic)? Answering these questions will help us engineer further on similar spin-chain systems, which has a strong potential to eventually lead to atomic-scale magnetic devices. I have also collaborated with the same STM group in probing the magnetic anisotropy of a single atom on a surface. This fundamental measurement has important technological consequences because it determines an atom's ability to store information. Previously, nobody had been able to measure the magnetic anisotropy of a single atom. This pioneering work on atomic-scale magnetic anisotropy was published at *Science* **317**, 1199 (2007). With further work it may be possible to build structures consisting of small clusters of atoms, or even individual atoms that could reliably store magnetic information. Such a storage capability would enable nearly 30,000 feature length movies or the entire contents of YouTube – millions of videos estimated to be more than 1,000 trillion bits of data – to fit in a device the size of an iPod. Perhaps more importantly, the breakthrough could lead to new kinds of structures and devices that are so small they could be applied to entire new fields and disciplines beyond traditional computing. This work has drawn attention of the general public, and received news coverage widely. *NBC TV news*, August 30, 2007, "IBM is using this microscope to put atoms to work storing our data. These are building blocks to increase storage capacity by a factor of 1,000 ... then you would need 1,000 less times fewer energy saving energy and room all in a very small package as real as you might imagine. IBM and other companies are working to head off what may be an impending limit to hard-drive capacities. The company's technique might help break through that limit, by suggesting a way to store information in single atoms." *Science Daily*, "major progress in identifying a property called magnetic anisotropy, which determines an atom's ability to store information. That research, said IBM, could lead to storage of as many as 30,000 movies in a device the size of an iPod." *Physics World*, "Physicists at IBM have developed a technique that could allow data to be stored in bits containing as little as one magnetic atom."

4. 研究方法

This project is a pioneering study of computational study in STM engineered atomic spins. Previous study of their inter-spin coupling using Mn has found the coupling being antiferromagnetic. However, only ferromagnetic coupling between atomic spins is suitable to build a cluster with a large total spin on surfaces, and such a large spin may eventually lead to spin device application. A straightforward trial for getting ferromagnetic coupling is to place Gd atoms on the CuN surface because Gd carries the largest atomic spin among all lathanoid atoms. Previous study of the anisotropy of a single Fe spin has found an anisotropy energy of about 1meV, which gives rise to tolerance of thermal energy of order 0.1meV=10K. For device applications of reasonable cooling cost, tolerance of thermal energy is expected to be 1~3meV=100~300K (liquid nitrogen to room temperature), which requires anisotropy energy of 10~30meV. Further enhancement of the anisotropy energy will bring such a single anisotropic spin closer to the real application. The lathanoid atoms Tb and Dy are good candidates of obtaining larger anisotropy energy on the CuN surface because of their relatively large L and S compared to Fe. Another way to enhance the anisotropy is to couple several anisotropic spins together. This approach requires preliminary study on the interplay between the spin coupling and will enable further development of giant magnetic anisotropy at the atomic scale.

During the three years, we will perform first-principles calculation of the electronic structures of magnetic atoms on CuN surfaces using Density Functional theory (DFT) in the Generalized Gradient Approximation (GGA) in the Full-potential Linearized Augmented Plane Wave (FLAPW) basis. Electronic-structure calculation of atoms and molecules, in particular Hartree-Fock theory and its descendants, was based on the complicated many-electron wavefunction. DFT's main objective is to replace the many-body electronic wavefunction (3N degrees of freedom for N electrons) with the electronic density (3 degrees of freedom in the space) as the basic quantity. Within the framework of the Kohn-Sham equation, the many-body interaction is reduced to an effective potential that includes the effects of the electron-electron Coulomb repulsion and the Pauli exclusion principles, e.g. the exchange and correlation interactions. It is difficult to find an exact form of the exchange-correlation potential. The simplest approximation is the local-density approximation (LDA), which is based upon exact exchange energy for a uniform electron gas. Most modern DFT codes now use more advanced approximations to improve LDA's accuracy. LDA uses the exchange-correlation energy for the uniform electron gas at every point in the system regardless of the inhomogeneity of the real charge density. This inhomogeneity can be expressed, to its lowest order, in terms of the gradient of the total charge density, well-known as GGA. For systems where the charge density is slowly varying, GGA has proved to improve LDA. Once the form of the exchange-correlation functional is determined, one needs a basis set to solve the Kohn-Sham equation. The most oscillating part of the electron wave function in a crystal is located close to the nucleus, but this region is quite shielded from the more outer regions of the atoms where chemistry happens, and the electrons are well described by atomic orbitals. In the region far away from the nuclei, the electrons are more or less free, and are described more efficiently by plane waves. Space is therefore divided into two regions: around each atom a sphere with radius is drawn as the muffin tin sphere, and the remaining space outside the spheres is called the interstitial region, as shown in Fig. 6. Within muffin tin spheres, the atomic orbitals are adapted, and in the interstitial region, the plane wave is used. This basis set is called Augmented Plane Wave (APW). The successors of the original APW, which linearize the orbital energy of the atomic orbitals to avoid solving the orbital energy transcendental equations and greatly improves the efficiency without loss of accuracy, are the Linearized Augmented Plane Wave (LAPW) family, e.g. LAPW,

LAPW+LO, etc.

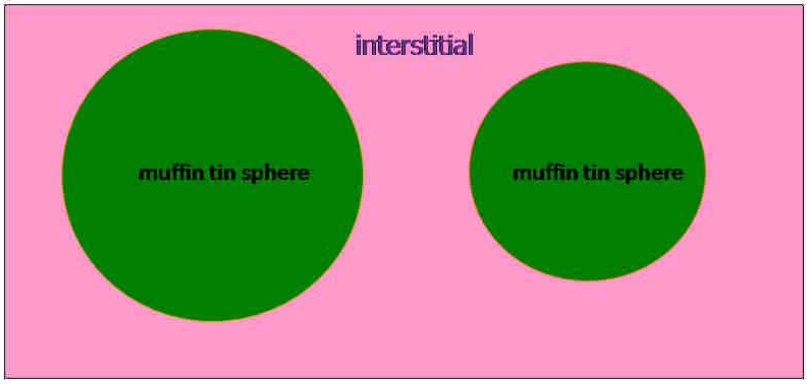

Figure 6: A unit cell is divided into the muffin tin spheres and the interstitial region when the APW basis is used.

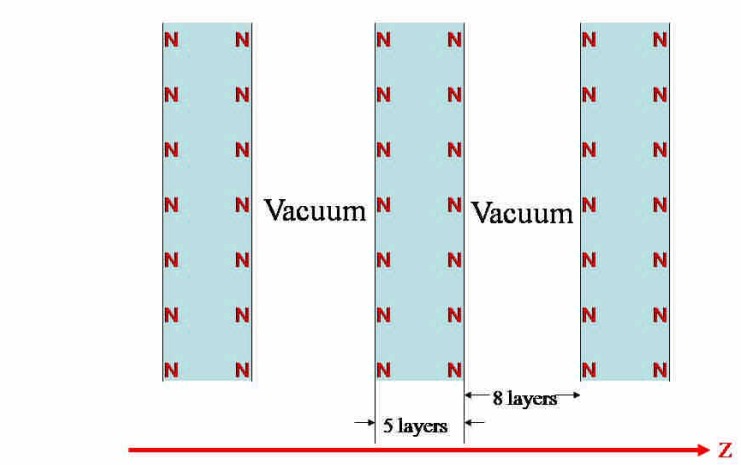

Figure 7: Periodic CuN slabs that simulate the CuN surface in my DFT calculation.

To simulate the Gd/CuN surface, we will first construct a CuN supercell of 5-layer slabs separated by 8 vacuum layers with the CuN monolayers on both sides of each slab and three Cu layers in between. During the first year, I will perform DFT-FLAPW calculation for one and two Gd atoms on CuN surfaces. In simulating a single Gd atom on CuN, we will place Gd atoms on top of the CuN surface at 10.80Å separation (Fig. 5 left). For Gd dimer, a 10.8 Å ×7.2 Å unit cell is used (Fig. 5 right). The atomic positions of this Gd/CuN surface will be optimized by using the Mn/CuN surface as the scratch structure, targeting the interatomic forces down to 10mRy-a_0. The structure optimization of the Gd dimer on the CuN surface will be performed with parallel Gd spins. The best-optimized structure will then be used to perform another DFT calculation with antiparallel spins because the exchange coupling of the Gd dimer will be calculated from the energy difference between the parallel- and antiparallel-spin configurations. In the case that the on-site Coulomb repulsion U of the Gd 4*f* orbital is large (>2eV), the GGA exchange functional can not work well for this particular orbital. This U can be calculated by the constraint GGA method. The way to recover this missing U in the conventional GGA functional is to apply the GGA+U method. The convergence of the self-consistent cycle can be poor in the presence of the well-localized 4*f* orbital.

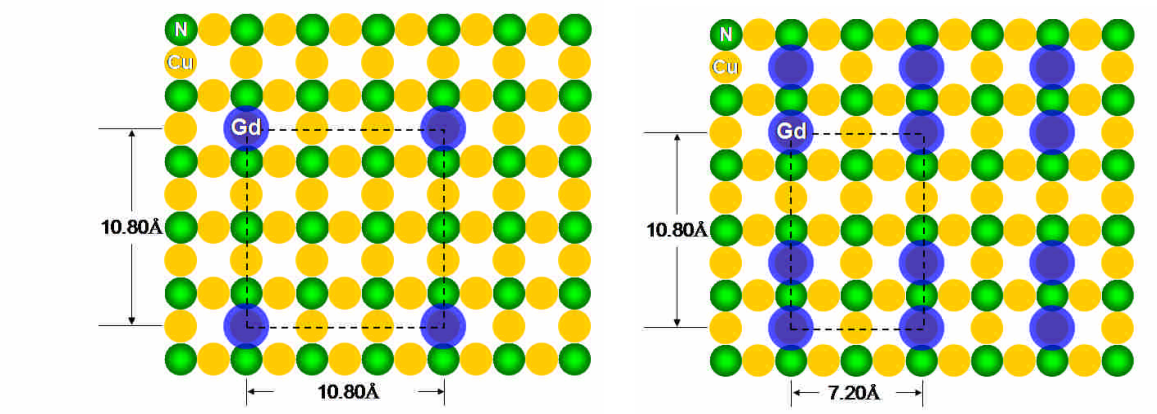

Figure 8: The top view of unit cells of a single Gd atom (left) and a Gd dimer (right) on the CuN surface to be used in this study.

During the second year, I will perform DFT-FLAPW calculation for a single Dy atom on the CuN surface. The bulk Dy is known to have a giant magnetic anisotropy. Its spin-orbit interaction is expected to be particularly large and also greatly enhanced compared with the previous anisotropy study using Fe atoms. A standard DFT-FLAPW calculation normally does not include the spin-orbit interaction. In such calculation the spin is not coupled to the lattice, and therefore it has no preferred direction. A system will exhibit magnetic anisotropy only when the spin-orbit interaction is considered. The classical explanation of spin-orbit coupling is that an electron moving with velocity $\boldsymbol{v} = \mathbf{p}/m$ in an external electric field $\mathbf{E} = -\nabla V(\mathbf{r})$ experiences a magnetic field given by the relativistic correction $\mathbf{p}/m \times (-\nabla V)/c$. Given a spherically symmetric potential $V(r)$ and accounting for the fact that the electron is spin-1/2, the interaction energy is then given by

$$H_{\mathrm{SO}} = \frac{e}{2m^2c^2r}\frac{dV}{dr}\mathbf{L}\cdot\mathbf{s}$$

The above equation is exact for spherical systems. In the FLAPW method the spin-orbit interaction is considered only within the muffin tin spheres, and the nonspherical potential is neglected when calculating dV/dr. The spin orientation is prescribed for a given DFT-FLAPW calculation, which gives rise to the total energy of the system of this particular spin orientation. By running calculations with the spin in the high-symmetry directions (in this project are x, y, z due to cubic symmetry), one obtains the energy differences among the symmetry axes. These energy differences represent the ability of flipping the spin to different directions, and are known as the spin anisotropy energy. To compare our calculated anisotropy energy to the STM-measured IETS spin excitation, the Hamiltonian of a single-spin in an anisotropic environment can be described, to lowest order, by

$$\hat{H} = D\hat{S}_z^2 + E\left(\hat{S}_x^2 - \hat{S}_y^2\right)$$

Physically, the best correspondence between the DFT-FLAPW calculation and the above spin Hamiltonian one can think of is to equal the DFT-FLAPW total energies of a i-direction spin ($i=x$, y, z) to the expectation values of the Hamiltonian in the $S_i = S$ spin states, up to a constant of the energy offset. The x , y, z three directions give three equations for the three unknowns D, E, and the energy offset, and hence D and E are solved from the DFT-FLAPW calculated total energies. On the other hand, STM measures the excitation

between different S_z eigenstates out of the IETS dI/dV steps, which also determines D and E. The calculated and measured values are compared to test the predictability of DFT-FLAPW calculation in spin anisotropy.

During the third year, I will perform DFT-FLAPW calculation for an Fe dimer on the CuN surface. The Fe dimer will be studied at both the Cu and the N sites. Previous studies were only concentrated on either

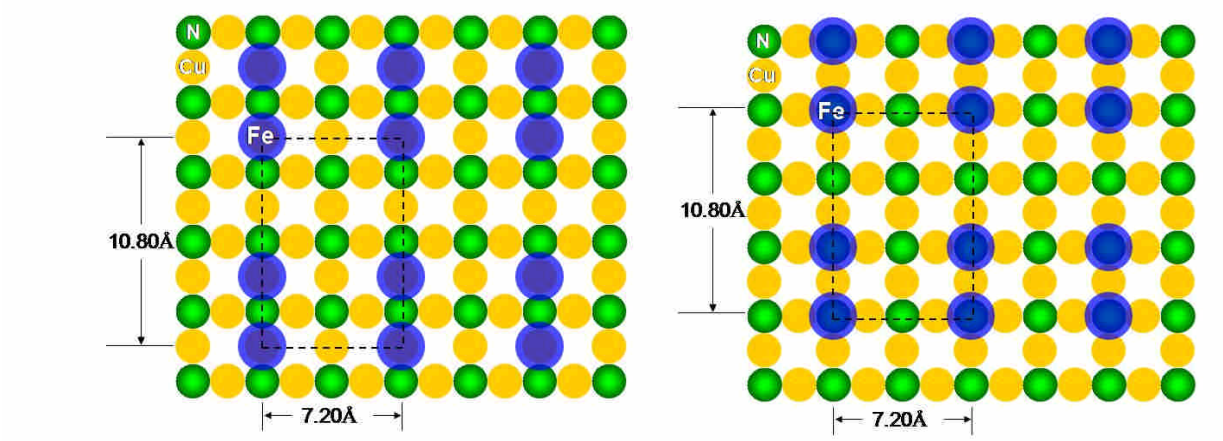

Figure 9: The top view of unit cells of the Fe dimer at the Cu site (left) and the N site (right) on the CuN surface to be used in this study.

the spin coupling (e.g. Mn chains) or the spin anisotropy (e.g. an Fe atom) at a time. Combining the spin anisotropy with the ability to couple atomic spins into extended quantum spin structures has the potential in completely engineering giant magnetic anisotropy at the atomic scale. The Fe dimer on the CuN surface serves as a simple system for studying the interplay of spin coupling and anisotropy. A model spin Hamiltonian that includes both the spin coupling and the anisotropy is given as follows

$$\mathcal{H} = \sum_{i>j} J_{ij}\mathbf{S}_i \cdot \mathbf{S}_j + \sum_i D_i(\hat{e}_i \cdot \mathbf{S}_i)^2$$

where the first term is the familiar Heisenberg Hamiltonian, and the second is the spin anisotropy term scaled with its corresponding constant D_i and depending on the orientation of each spin $\mathbf{S}_i$ relative to the anisotropy easy axis of that spin. The advantage of first-principles calculation to the extraction of coupling and anisotropy parameters is that spin-orbit interaction can be switched on and off in a fully controllable way. This allows us to first run a calculation without the spin-orbit interaction of Fe, which corresponds to the model spin Hamiltonian with D=0. The atomic spins of a system can generally be assigned in arbitrary relative orientations to perform DFT calculation. A special subset of these orientation configurations is called to be collinear when spins are either parallel or antiparallel to each other. We will first perform DFT-FLAPW calculations to optimize the relaxed structure of the Fe dimer on the CuN surface. The best-optimized structure will then be used to perform another DFT calculation with antiparallel spins because the exchange coupling of the Fe dimer will be calculated from the energy difference between the parallel- and antiparallel-spin configurations. Once the coupling J is determined, the Fe anisotropy parameter D can be calculated by switching on the spin-orbit interaction. We will calculate the DFT-FLAPW total energy of the parallel-spin orientation with the spin-orbit interaction included. The difference between this total energy and that with the same spin orientation but no spin-orbit is the anisotropy parameter D multiplied by the square of the Fe spin, from which D can be determined. The Fe dimer can be placed either at the Cu or N binding site, and the structure relaxation and the parameter extraction will be repeated for both sites. The spin coupling and anisotropy of placing Fe at these two sites will be compared. We will also look for a qualitative interpretation

of the difference between these two cases by inspecting the Fe's binding nature to the CuN surface. The spin couplings of Fe and Mn dimers will also be compared.

All computing jobs were performed on the eight computing servers funded by this grant.

5. 結果與討論

The first-year project is the study of Gd dimers on the CuN surface. We perform first-principles calculation of the Gd adatoms on the CuN surface. On one hand, the Gd atoms are similar to the previously-studied Mn atoms when being deposited on the Cu sites of the CuN surface, i.e., the Gd's nearby N atoms break bounds with their neighboring Cu and form a "quasi" molecular structure from the surface. On the other hand, the local structures of the Gd atoms on the CuN surface have a wellstudied reference system, the GdN bulk. We build two different geometries of the Gd dimers on the surfa- ce: one has Gd atoms along the same N row, and the other along two perpendicular N rows. The two geometr- ies mimic the coupling paths of the nearest-neighbor (NN) and next-NN Gd atoms of the GdN bulk, where two paths in bulk have ferromagnetic and antiferromagnetic couplings, respectively. We calculate the exchange couplings J of two arrangements of Gd2/CuN using first-principles PBE+U, and expect that one of the two types of surface Gd dimers will exhibit ferromagnetism and the other antiferromagnetism.

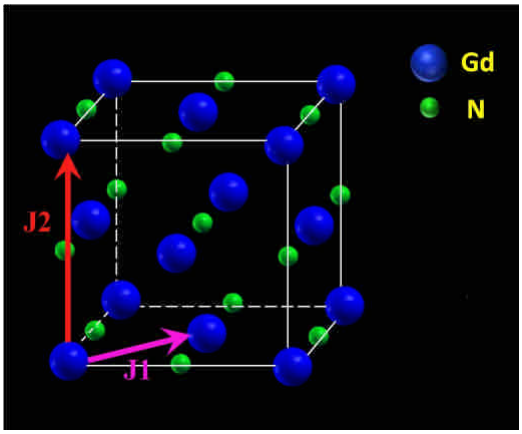

Figure 10: The unit cell of a GdN bulk. The Gd-to-Gd arrows indicate the NN (diagonal, purple) and next-NN (linear, red) couplings.

In the scanning tunneling microscope (STM) experiments, a copper-nitride monolayer is built between a magnetic atom and the Cu(100) surface to keep the atomic spin away from the screening of its underlying conduction electrons while to per-mit a sufficient amount of STM tunneling current for probing the spin excitations. To understand the magnetic properties of Gd atoms on the CuN surface, we simulate a single Gd on this surface by first constructing a supercell of 5-layer Cu slabs plus 8 vacuum layers with the nitrogen atoms snugging in-between the half of vacant sites and then placing each Gd atom on top of the CuN surface within 3 unitcells of the CuN surface. We perform density-functional calculations in the all-electron full-potential linearized augmented plane wave (FLAPW) basis. A naive local density approximation (LDA) or generalized gradient approximation (GGA), when being applied to materials composed of rare-earth atoms, generally yields f levels inconsistent to photoemission experiments, and needs to be fixed by adding extra on-site Coulomb repulsion to the exchange-correlation functional, the so-called DFT+U method. To determine the on-site Coulomb U_f and exc- hange J_f values of the Gd 4f orbitals on the CuN surface, we revisit the GdN bulk system, which mimics very well the local structure of Gd on the CuN surface. Following the same way as the previous LSDA+U studies, we find that U_f = 11 eV and J_f = 2 eV yield the majority spin 4f level in the best agreement with photoemission measurements. This set U_f and J_f are used in our succeeding

calculations of both the GdN bulk and the Gd dimer on the CuN surface. The spin couplings along the diagonal and the linear Gd-N-Gd paths of the GdN bulk are well-studied in the literatures, where the two Gd atoms along the paths are NN and next NN to each other, respectively. The two coupling paths between Gd atoms in a GdN bulk strongly suggest that two possible geometries of Gd dimers on the CuN surface: one has Gd-N-Gd along the N row, and the other in a right angle (two Gd atoms along the diagonal).

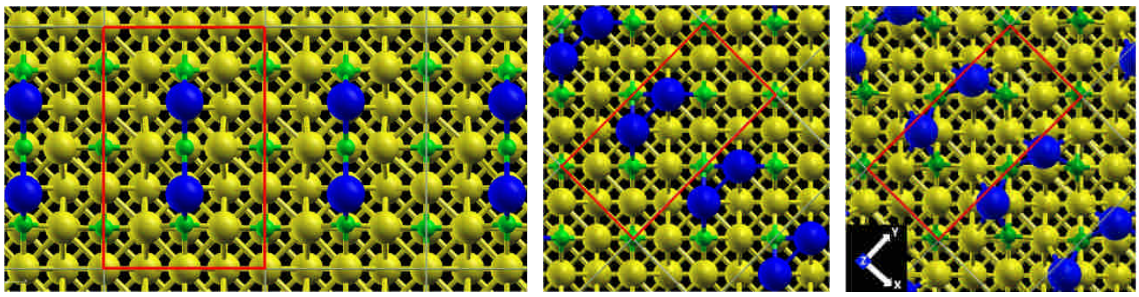

Figure 11: The left figure is the top view of the relaxed structure of a linear Gd dimer on the CuN surface. The center and right figure shows the top view of the initial and relaxed structure of a diagonal Gd dimer on the CuN surface. Unit cells are marked by red rectangles.

	Gd to Gd	Gd-N	∠ Gd-N-Gd	*J* (mev)
NN Gd In GdN bulk	3.52 Å	2.49 Å	90°	-0.14 (-0.29)
Next NN Gd inGdN bulk	4.98 Å	2.49 Å	180°	0.29 (0.15)
Diagonal Gd dimer On CuN surface	3.64 Å	2.19 Å	112°	-1.27
Linear Gd dimer On CuN surface	4.15 Å	2.24 Å	135°	0.177

Table I: Calculated Gd-to-Gd distances, Gd-N bond length, Gd-N-Gd bond angle, and the spin coupling *J* between Gd of four systems. The *J* values within parentheses are deduced from the measured N_eel and Curie temperatures.

Previous studies have concluded that the spin couplings between Gd atoms of a GdN bulk along the diagonal and the linear paths are ferromagnetic and antiferromagnetic, respectively. Therefore we expect the Surface Gd dimers in two geometries to have spin couplings same as their counterparts of similar geometries in the GdN bulk, i.e. diagonal (linear) being ferromagnetic (antiferromagnetic). We therefore arrange Gd atoms in such two geometries on the CuN surface, and optimize the crystal structures until the maximum force among all the atoms reduces to $\lesssim 10$ mRy$/a_0$ and 5 mRy$/a_0$. The relaxed structures are shown in Fig. 11, and the dimer local geometries are quantitatively presented in Table I. It is interesting to notice that the diagonal Gd dimer relaxes its its bond angle from 90° to 112°. This can be understood in the way that the diagonal Gd-to-Gd distance in GdN bulk is 3.52Å, and the initial Gd-Gd distance on the surface is 2.56Å, much shorter than 3.52Å, so the relaxed Gd-Gd distance on the surface 3.64Å is rather reasonable. To determine the Gd spin on the CuN surface, we plot the calculated density of states of a single Gd on this surface in Fig. 12. One clearly sees that the 4*f* majority spin states are all occupied and the minority states are all unoccupied, which implies a $4f^{7}$ configuration for Gd, a spin -7/2 configuration for its 4*f* shell. Besides, the 5*d* states are completely absent, in contrast to a free Gd atom that carries a valence configuration $5d^{1}4f$

$^7 6s^2$.

To calculate the spin coupling J between Gd spins on the CuN surface, we take advantage of the correspondence between the collinear spins of a Heisenberg model and the magnetic moments of the real crystal surface of interest. The Hamiltonian of a Heisenberg spin dimer is

$$H = JS_1 \cdot S_2 \tag{1}$$

The difference of energy expectation values δE between the parallel and antiparallel spins is related to the coupling J, for spin-S atoms, as

$$\delta E = JS^2 - \left(-JS^2\right) = 2JS^2 \tag{2}$$

To calculate the total energy of a Gd dimmer on the CuN surface, we simulate the system by the same slab setup as the single Gd except that the Gd atoms on the surface are arranged within 3 unitcells of the CuN surface. By calculating the total energies of the paralleland antiparallel-spin configurations of a Gd dimer at the Cu site of a CuN surface, we obtain from (2) the exchange coupling J to be 0.177 meV for the linear dimer and -1.27 meV for the diagonal dimer. Our calculations obtain a weakly anitferromagnetic Gd dimer of the linear dimer and ferromagnetic of the diagonal dimer, with each dimer sitting on the CuN surface.

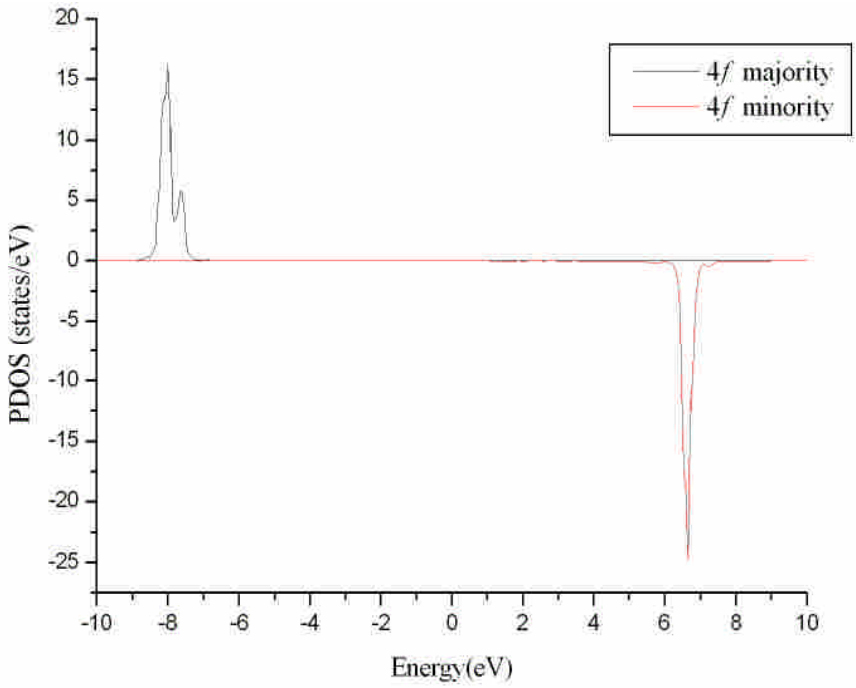

Figure 12: PDOS of the a single Gd on the CuN surface.

We now turn our attention to the underlying mechanism of the ferromagnetism of the diagonal Gd dimer. There are three possible magnetic interactions that may couple the two Gd spins, the direct exchange, the superexchange, and the Ruderman-Kittel-Kasuya-Yosida (RKKY). To extract the three components out of the resultant ferromagnetic coupling, we perform calculations of two modeled systems. One is the original Gd dimer on the surface with the the in-between N atom removed, which essentially has the superexchange turned off. The other is a Gd dimer on top a single CuN layer, i.e., removing the underlying metallic Cu(100) slab with the dimer and CuN sheet remained, which has basically no RKKY. We then decompose the spin

couplings of the three systems, the original Gd dimer on the CuN / Cu(100) surface J , the one without the N in between two Gd atoms J_α, and the Gd dimer on a single CuN sheet J_β, into the contributions of direct exchange J_d, superexchange J_s, and RKKY J_r. We write down their relations as

$$\begin{aligned} J &= J_d + J_s + J_r \\ J_\alpha &= J_d + J_r \\ J_\beta &= J_d + J_s \end{aligned} \tag{3}$$

J	J_α	J_β	J_d	J_s	J_r
-1.27	-1.62	-1.31	-1.66	0.35	0.038

Table II: Calculated spin couplings in meV of the original diagonal Gd dimer on the CuN/Cu(100) surface J, the one without the N in between two Gd atoms J_α, and the Gd dimer on a single CuN sheet J_β. Also listed are direct exchange J_d, superexchange J_s, and RKKY J_r extracted out of J , J_α, and J_β.

The calculated spin couplings are listed in Table II. The insignificant differences among J , J_α, and J_β imply that the N atom in between and the underlying conduction electrons play minor roles in the spin coupling of the diagonal Gd dimer, while the direct wavefunction overlapping between the two Gd atoms actually dominates. In fact, the obtained J_d, J_s, and J_r values reflect the statement above, where the super exchange and RKKY are 21% and 2.3% of the direct exchange, respectively.

In summary, we have calculated the electronic structures of the coupled rare-earth (Gd) spins on a surface using the PBE+U exchange correlation. The precise positions and atomic charges of those systems, unlikely accessible by experimental techniques, are determined by structure relaxation and Bader analysis respectively in our calculations. The charge analysis shows that the GdN bond formed by the Gd-deposited CuN surface has stronger bond polarity than the Cu-N bond. The presence of Gd gives rise to rearrangement of the atomic structure that is quite different from what a Mn atom does. The calculated $J's$ of the Gd dimers along the N row and the diagonal are antiferromagnetic and ferromagnetic, showing that the sign of J can be tuned by different geometric arrangements. The underlying physics of the ferromagnetism of the diagonal dimer is studied by decomposing its contributions into the direct exchange, superexchange, and RKKY.

The second-year project is the study of a single Dy atom on the CuN surface. As already pointed out in the previous Fe study, when an adatom is deposited onto the Cu site of the surface, it establishes polar covalent bonds with the nearest-neighbored N atoms that replaces the original CuN binding network. The calculated electron density of a Dy atom in the CuN surface is shown in Figure 13a, together with the previously calculated Fe re-presented. As one can see, the Dy atom, sitting even higher on top of the surface, attracts its neighboring N atoms further out of the surface than the Fe case. We have also calculated that Dy and its neighboring N are +1.3 and −1.2 charged respectively. Compared with the +0.9 and −1.4 charged Fe and its neighboring N respectively, the Dy-N bond of the Dy system has a polarity approximately the same as the Fe-N.

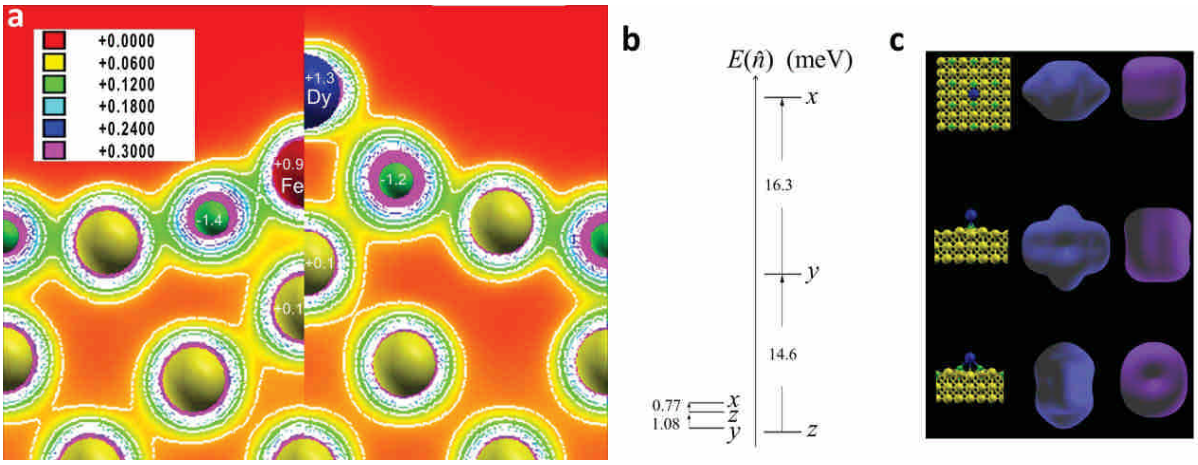

Figure 13: (a) Electron density contour of a single Dy on the CuN surface along the N-Dy-N raw and the out-of-plane direction, in comparison with the Fe case. The green and yellow circles are N and Cu atoms, respectively. The numbers inside the circles indicate the net charge on selected atoms. (b) Level diagrams in scale showing the calculated MAE of Fe (upper) and Dy (lower) on the CuN surface, respectively. The Fe case is done by Shick *et al. Phys. Rev.* B, **79**, 172409 (2009). (c) Calculated spin-density isosurfaces (second column, blue) for Dy on CuN at the magnitude of $0.05\, e / a_0^3$ within a 3×3×3 Å^3 cube centered at the Dy nucleus, by looking (top to bottom) from the top, along the N row, and along the hollow direction. The stick-ball structures are the corresponding structure views in these three directions. The purple surfaces are the corresponding Fe spin density for comparison.

By pointing the Dy spin in the hollow, N-row, and out-of-plane three symmetry directions (to be called *x*, *y*, and *z* respectively) in our density-functional-theory (DFT) total-energy calculations with spin-orbit couplings (SOC) included, we obtain the Dy magnetic anisotropy energy (MAE) $E(\hat{n})$ of $\hat{n} = \hat{e}_x$, $\hat{e}_y$, and $\hat{e}_z$, and compare it with the Fe case, as shown in the level diagram in Figure 13b. One notices that in contrast to the Fe case, the most-preferred magnetization axis of Dy is oriented in the out-of-plane direction, while two atoms both have their least-preferred axis pointing in the hollow direction. The calculated least-preferred axis of both atoms will be understood, in a later discussion, in a simple picture using analysis of localized orbitals, the Dy 4*f* and Fe 3*d*. The MAE of Dy is basically one order of magnitude larger than that of Fe, and is five times larger than the 6meV MAE of Co on the Pt surface, the largest single-atom MAE reported previously.

The previously studied Fe on the surface has 13.5% of spin density extends into the surrounding atoms with the spreading primarily along the N-row direction. In contrast to Fe, when calculating Dy on the same surface, we find that a net spin of *S*=2.94 is localized at the Dy atom, and *S*=2.91 by including the spin of all atoms, indicating that there is no spin spreading, and the spins of the atoms surrounding Dy are slightly negatively polarized. The Dy atom with *S* = 2.94 essentially behaves like a Dy^{+2} ion, and analysis of its partial density of states (PDOS) shows a valance electronic configuration $(4f)^9(6s5d)^1$, where PDOS of 4*f* is analyzed in a latter paragraph, and 6*s*5*d* denotes a hybridized molecular orbital. The significant reduction of spin spreading when replacing Fe by Dy is obviously because the Dy 4*f* orbitals are more localized than the Fe 3*d*. Another interesting feature is the shape of the spin density. When looking closely at the spin isosurfaces of the Dy and Fe atoms along all three crystal-symmetry directions in Figure 13c, the shapes of Dy and Fe are found to be approximately a hexagon and a square, respectively, along either the N-row or out-of-plane direction, while both atoms become more round-shape-like along the hollow. This seemly mysterious observation of spin shapes will become clear when we later look into the Fe 3*d* and Dy 4*f* orbitals in the CuN surface.

The *d* orbitals in a crystal environment have the following well-known subshell symmetries, z^2, x^2-y^2, *xy*,

yz, *zx*. The exotic, complicated *f* orbitals, which are rarely shown in literatures, have two commonly used sets of subshell symmetries, the cubic and the general sets. Here we propose an unconventional set of *f* orbitals such that six of the orbitals have fully polarized angular momenta, as one will see its advantages in the orbital analysis of SOC and spin shapes. Five out of the seven orbitals, xz^2, yz^2, $y(3x^2-y^2)$, $x(x^2-3y^2)$, and xyz belong to the general set. The rest two are $z(z^2-3x^2)$ and zy^2, which are related to the general-set orbitals z^3 and $z(x^2-y^2)$ simply by the following orthogonal transformation

$$\begin{pmatrix} |x'(x'^2-3y'^2)\rangle \\ |x'z'^2\rangle \end{pmatrix} = \begin{pmatrix} |z(z^2-3x^2)\rangle \\ |zy^2\rangle \end{pmatrix} = \frac{1}{4}\begin{pmatrix} \sqrt{10} & -\sqrt{6} \\ \sqrt{6} & -\sqrt{10} \end{pmatrix}\begin{pmatrix} |z^3\rangle \\ |z(x^2-y^2)\rangle \end{pmatrix} \quad (4)$$

where the primed coordinates are arranged as $(x', y', z') = (y, z, x)$. It can be seen that $z(3y^2-z^2)$ and zx^2, which are orthogonally transformed from the general-set $z3$ and $z(x^2-y^2)$, no longer belong to the general set in the unprimed coordinates, but are actually the general-set orbitals $x'(x'^2-3y'^2)$ and $x'z'^2$ in the primed coordinates. One can easily verify that each orbital of this set except for *xyz*, with its quantization axis $\hat{n}$ properly chosen along one coordinate axis, has its angular momentum fully polarized, that is, they are eigenstates of $|\mathbf{L}\cdot\hat{n}|$ with eigenvalues $|m| = 3 = l$. The full polarization of $|\mathbf{L}\cdot\hat{n}|$ of these six 4*f* orbitals can be further visualized clearly by looking at their orbital shapes. As one can see in Figure 14a, the above mentioned six fullypolarized 4*f* orbitals have an unique six-petal shape, and can be grouped into three pairs. Each pair of orbitals have the same coordinate axis as their central symmetry axis, and are related to each other by exchanging their in-plane axes. The most obvious full polarization can be realized for the $y(3x^2-y^2)$ and $x(x^2-3y^2)$ orbitals, which are eigenstates of $|L_z|$ with eigenvalues $|m| = 3$, and have *z* as their central axis. Similarly, each of the rest four fully-polarized orbitals have their central axes as their polarization directions. The only exception, the *xyz* orbital, has eight lobes pointing to the corners of a cube.

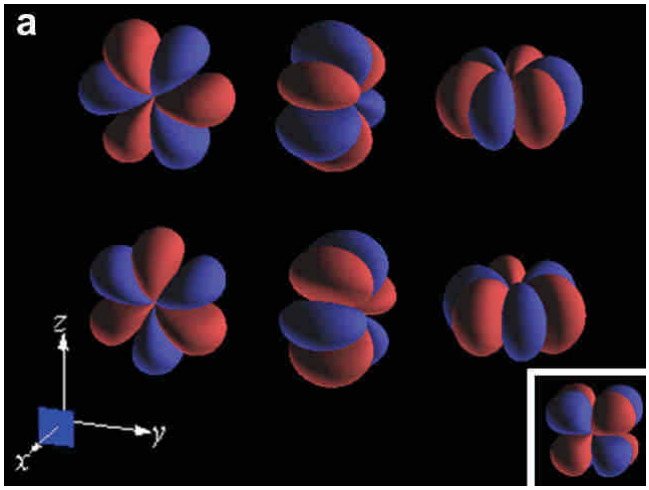

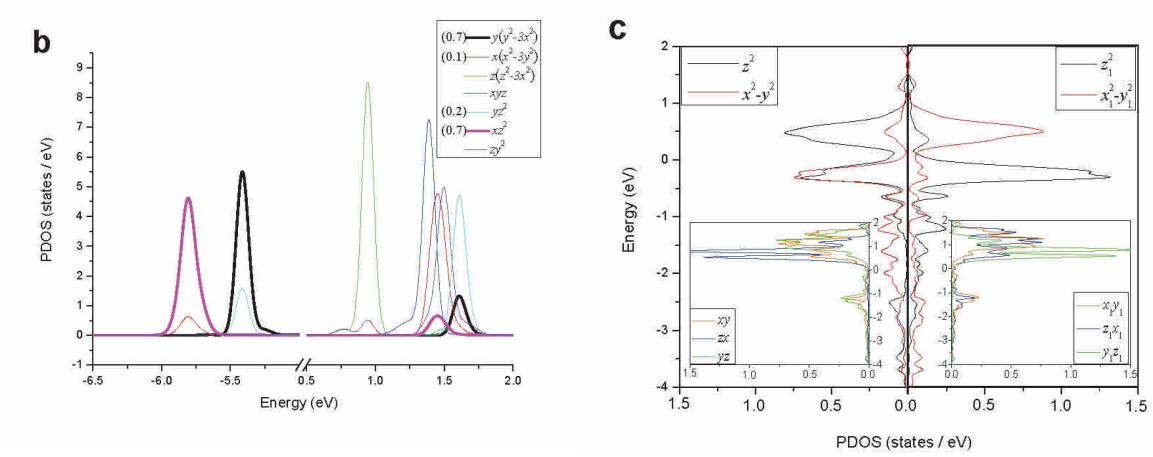

Figure 14: (a) Schematic plots of L-fully-polarized 4*f* orbitals, where blue (red) zones denote positive (negative) values. From left to right: (upper) yz^2, $z(z^2-3x^2)$, $x(x^2-3y^2)$, (lower) zy^2, xz^2, $y(3x^2-y^2)$. All six orbitals have a unique six-petal shape. The only exceptional shape of the *xyz* orbital is plotted in the inset at the right-lower corner. (b) The 4*f* minority-spin PDOS of Dy on the CuN surface. The subshells follow the choice of Figure 14a. The nontrivial occupation are specified in parentheses. (c) The 3*d* minority-spin PDOS of Fe on the CuN surface. The left figure has the conventional quantization axes with the hollow, N-row, and out-of-plane directions being *x*, *y*, and *z* axes, respectively. In contrast to the conventional set of axes, the right one has unconventional axes $(x_1,y_1,z_1)=(y,z,x)$, and is used to perform orbital analysis in this work for its simple occupation numbers (either nearly occupied or almost empty). The PDOS of three of the subshells are plotted separately in each inset solely for the purpose that all PDOS are better visualized.

Our calculations show that the Dy 4*f* majority-spin states are all fully occupied and are very low-lying, extremely atomic-like levels. Instead of plotting PDOS, their majority-spin energy levels are shown in Table1, together with their weights in the L-fully-localized 4*f* orbital basis. The orbital analysis of this work does not depend on the details of the Dy 4*f* majorityspin states as long as all of them are fully occupied, and their details are not presented here. For minority-spin states, we plot their PDOS in Figure 14b, and find that xz^2 and $y(3x^2-y^2)$ are mainly occupied, and yz^2 and $x(x^2-3y^2)$ slightly occupied. The occupation numbers of the rest of the 4*f* minority-spin states as well as the 5*d* and 6*s* (see Supplemental I) are negligible. The Dy 4*f* orbitals are rather localized as indicated from a previous paragraph that they have an approximate 0.4 Å radius. It is a good approximation to think of these orbitals in the way of electronic configurations of an atom, and therefore the nontrivial occupation (neither fully occupied nor completely empty) is determined for each orbital from the area under the curve below the Fermi level. The PDOS thus implies an approximately $4f^{9}$ configuration for the Dy atom itself.

The conventional quantization axes of the Fe 3*d* PDOS are oriented in the way that the *x* axis points along the hollow direction, *y* along the N row, and *z* out of plane. Such PDOS have been presented in Shick *et al. Phys. Rev.* B, **79**, 172409 (2009) and show that all the majority-spin states are fully occupied. We re-calculate the PDOS and plot the minority spins in Figure 14c. The minority-spin PDOS show that x^2-y^2 is fully occupied, z^2 partially occupied, and the rest three minority-spin states basically empty. The partially occupied spin-minority z^2 prohibits us from establishing a simple picture of either the spin-density shape or the SOC. However, one may notice that the z^2 and x^2-y^2 PDOS profiles depend nontrivially on the choice (or interchange) of the coordinate axes, while the *xy*, *yz* and *zx* (see the insets of Figure 14c) have trivially the same set of PDOS profiles with interchange of PDOS labels corresponding to the interchange of the

coordinate axes. Therefore we search for z^2 and x^2-y^2 minority-spin PDOS of all three possible assignments of coordinate axes, i.e., the hollow, N-row, and out-of-plane directions are *x*, *y*, and *z* axes, respectively, and the cyclic permutations. In all three axis assignments, all the majority-spin states are always fully occupied, and the *xy*, *yz* and *zx* minority-spin always empty, while the z^2 and x^2-y^2 minority-spin states have specially simple occupations as shown in Figure 14c under a particular assignment of new axes: the hollow, N-row, and out-of-plane directions are z_1, x_1, and y_1 axes, respectively. In this new coordinate system, only the z_1^2 (or equivalently x^2 in the old coordinates) orbital has paired spins, while the rest four all unpaired.

With the orbital quantum numbers and occupation numbers determined, we first try to explain the spin-density shape of a Dy atom on the CuN surface. By starting with the top view, one notices that the $x(x^2-3y^2)$ and $y(3x^2-y^2)$ orbitals both have the six-petal shapes centered about the zaxis. As we have identified from the PDOS analysis that $y(3x^2-y^2)$ has roughly paired spins, while $x(x^2-3y^2)$ has roughly an unpaired spin. The spin density shape along the *xy* plane are therefore dominated by the $x(x^2-3y^2)$ majority spin along. Observing the shape of the $x(x^2-3y^2)$ orbital, one then realizes that the hexagonal shape of the Dy spin density from a top view in Figure 13c is essentially the consequence of the unpaired $x(x^2-3y^2)$ orbital. Similarly, the $z(z^2-3x^2)$ and xz^2 orbitals, both with a six-petal shape centered about the *y*-axis, contribute to the hexagonal spin density by looking along the *y* direction. However, the yz^2 and zy^2 orbitals, centered about the *x*-axis, both have unpaired spins. Their two six-petal shapes with 30° relative to each other result in a slightly-round-shape spin-density by looking along the *x* direction.

The orbital analysis not only can explain the shape of the spin density, but can also determine, as we are going to show, the spin orientation with the largest SOC. In DFT total-energy calculations, the magnetic anisotropy along symmetry axes are determined by pointing the Dy spin in these axes (or more accurately speaking, pointing the magnetization of the unit cell) with SOC included. Since the Dy spin is dominated by its 4*f* orbitals, we decompose the SOC contribution coming from each of the seven 4*f* orbitals, and estimate $|\mathbf{L}\cdot\mathbf{s}|$ from each orbital. First of all, the *xyz* orbital has a cubic symmetry, and contributes the same amount of SOC no matter which symmetry direction the spin points to. This means that one does not need to take the *xyz* orbital into account in comparing the MAE along different symmetry axes. We start by pointing the Dy atomic spin along the *x* axis. There are two *x*-polarized orbitals, yz^2 and zy^2, both mainly spin unpaired. Each of these two unpaired electrons contributes an amount of $(n\uparrow-n\downarrow)|\mathbf{L}\cdot\mathbf{s}|=|\mathbf{L}|\hbar/2$, where $\hbar=2$ is simply the unpaired spin of each orbital. The angular momenta L of the four other six-petal orbitals point in the *y* and *z* axes, which are all perpendicular to their *x*-oriented spins, and contribute no SOC. Therefore, the six six-petal orbitals contribute a total amount of $|\mathbf{L}\cdot\mathbf{s}|=|\mathbf{L}|\hbar$. Similar analyses of pointing the Dy spin in the *y* and *z* axes both yield $|\mathbf{L}\cdot\mathbf{s}|=|\mathbf{L}|\hbar/2$, respectively. The above $|\mathbf{L}\cdot\mathbf{s}|$ estimation concludes that the SOC reaches its largest value when the Dy spin points to the hollow direction (*x* axis). Observing the MAE obtained by the DFT total-energy spin-orbit calculation in Figure 13b, the least-preferred spin orientation (the highest MAE) also points along the hollow direction. Therefore, the simple $|\mathbf{L}\cdot\mathbf{s}|$ estimation explains how the leastpreferred axis of magnetic anisotropy forms, provided that the SOC contribution is positive. The positive sign of the Dy SOC is consistent with a recent quantum-chemistry, complete active space self-consistent field calculation (CASSCF) of a $DyCl_3$ molecule.

The simple occupation picture of the adatom's localized orbitals that explains both the spindensity shape and the least-preferred axis of magnetic anisotropy works not only for the rare-earth atom Dy. As we are going to show below, the same picture also works for the previously studied Fe adatom. When showing the Fe

PDOS in both the conventional quantization axes (hollow x, N-row y, and out-of-plane z) and the unconventional ones (hollow z_1, N-row x_1, and out-of-plane y_1) in Figure 14c, we have demonstrated that in the new coordinate system (x_1, y_1, z_1), only the z_1^2 (or equivalently x^2 in the old coordinates) orbital has paired spins, while the rest four are all unpaired. The square spin-density shapes of Fe in the CuN surface from the top view and N-row side view are essentially consequences of the spin-unpaired z_1x_1 and y_1z_1 orbitals, respectively, while the round shape from the hollow-site side view is the combination of the spin-unpaired $x_1^2 - y_1^2$and x_1y_1 orbitals. One also notices that $x_1^2 - y_1^2$ and x_1y_1 both have their **L** pointing in the z_1 (hollow) direction, and y_1z_1 and z_1x_1 in the x_1 (N-row) and y_1 (out-ofplane) directions, respectively. By a $|\mathbf{L} \cdot \mathbf{s}|$ estimation similar to the Dy case, we conclude that the SOC contribution reaches its largest value when the Fe spin points to the hollow direction (x axis). Observing the Fe MAE obtained by the DFT total-energy spinorbit calculation as shown in Figure 13b, the highest MAE also points along the hollow direction. Therefore, the simple $|\mathbf{L} \cdot \mathbf{s}|$ estimation again explains how the least-preferred axis of magnetic anisotropy forms for Fe, provided that the SOC contribution is positive. The positive sign of the Fe SOC is consistent with a recent quantum-chemistry calculation of molecules with 5*d* and 6*d* transition metal ligand bonds.

The scanning tunneling microscopes (STM) moving-atom technique has demonstrated its capability of building, manipulating, and measuring a single atomic spin in a well-characterized environment. First-principles calculations conclude that such an atomic spin forms a surface-embedded molecular magnetic structure, as well as, reproduce the measured magnetic anisotropy axes. As an ongoing study of the STM-engineered adatoms, this work is the first attempt to understand the magnetic anisotropy of a sur-face magnetic atom in a simple, atomic-scale microscopic picture. This is achieved by analyzing the occupations, shapes, and angular momenta of its individual localized orbitals. These localized orbitals include both the well-known *d* orbitals of the transition-metal atoms and the nontrivial *f* of the rare-earth. We determine an unconventional set of 4*f* subshell quantum numbers that can be used to analyze the spin density and the magnetic-anisotropy axes. The spin-density shape of a magnetic adatom is explained by simply counting the occupation of each individual subshell and spin state of the atom's localized orbital. The formation of the least-preferred magnetization axis is understood by simple estimation of adding up the $|\mathbf{L}\cdot \mathbf{s}|$ contributions from individual localized orbitals. These studies provide an important microscopic picture of the atomic-scale origins of magnetocrystalline anisotropy and magnetization distribution. We have also done the first study of a single rare-earth atom in a surface, computationally. The calculation predicts a record-high MAE of 31 meV.

The third-year project is the study of Fe dimers on the CuN surface. We perform first-principles calculation of the Fe adatoms on the CuN surface. The Fe atoms are similar to the previously-studied Mn atoms when being deposited on the Cu sites of the CuN surface, i.e., the Fe's nearby N atoms break bounds with their neighboring Cu and form a "quasi" molecular structure from the surface. We build both Fe atoms of this dimer at the Cu site of the surface. Following the previous studies of molecular magnets and surface engineered spins, we employ a model spin Hamiltonian to describe a spin dimer with its individual atoms carrying magnetic anisotropy.

$$H = J_x\, S_{1x}S_{2x} + J_y\, S_{1y}S_{2y} + J_z\, S_{1z}S_{2z} + D(S_{1z}^2 + S_{2z}^2) + E(S_{1x}^2 - S_{1y}^2 + S_{2x}^2 - S_{2y}^2) \qquad (5)$$

where the x, y, and z are the hollow, out-of-plane, and N-row three directions, respectively, and J_x, J_y, and J_z are spin exchange couplings of an anisotropic Heisenberg Hamiltonian, and D and E are the anisotropic

constants up to the nonvanishing, lowest order in the spin operators. The most important results we have achieved is to extract these constants out of the DFT calculations. By simultaneously considering the parallel and antiparallel spins and the three spin orientations (crystal symmetry directions) of the spin-orbit couplings, we obtain six DFT total energy values, i. e., five energy differences. These five energy differences correspond to the expectation values of energy differences of our model spin Hamiltonian in corresponding $|\mathbf{S}_1, \mathbf{S}_2\rangle$ states. Such correspondence between DFT spin configurations and model spin states provide us a set of simple algebraic equations so that we can extract the constants J_x, J_y, J_z , D, and E as listed in Table III

	J_X	$J_y = J_Z = J_{yz}$	D	E
Fe dimer	19.6	19.9	-0.44	-0.05
Fe dimer (no spin-orbit)	19.7			
Single Fe			-0.36 (-1.55)	0.10 (0.31)

Table III: Calculated anisotropic Heisenberg exchange couplings J_x, J_y, and J_z and anisotropic constants D and E in meV of an Fe dimer on the CuN/Cu(100) surface. The Fe dimer without spin-orbit coupling exhibits an isotropic Heisenberg model. The anisotropy constants of a single Fe on the same surface is listed for comparison, with STM-measured values in parentheses.

One see that the Heisenberg exchange couplings are uniaxial about the x (out-of-plane) direction. Compared with the isotropic exchange coupling when spin-orbit coupling is turned off, J_x decreases by 0.5% while J_{yz} increases by 1%. If we compare the dimer's anisotropy constants with those of a single Fe atom, we find that D maintains its sign and increases 22% in magnitude, and E changes its sign from positive to negative. More analysis is undergoing for this Fe-dimer study at the time we are writing this report.